ELSEVIER

Journal of Neuroscience Methods 103 (2000) 191–197

JOURNAL OF NEUROSCIENCE METHODS

www.elsevier.com/locate/jneumeth

Surface fractal computation and its application to immunofluorescent histochemical studies of calpain and calpastatin in PC12 cells

Paolo B. DePetrillo *, Qingfeng Yang, Jamie Rackoff, Anitza SanMiguel, Kamran Karimullah

Unit of Clinical and Biochemical Pharmacology, Laboratory of Clinical Studies, Division of Intramural Clinical and Biochemical Research, National Institute on Alcohol Abuse and Alcoholism, National Institutes of Health, Building 10 Room 3c-103, 10 Center Drive MSC 1256, Bethesda, MD 20892-1256, USA

Received 23 March 2000; received in revised form 15 August 2000; accepted 15 August 2000

Abstract

The purpose of this report is to present a method which can be used to parameterize patterns of immunofluorescent staining in cultured neural cells. The algorithm is based on the observation that the variance in pixel intensity of the image is a power function of the magnitude of the area in immunofluorescently stained PC12 cells. This property is used to derive the fractal dimension (D) of the region of interest (ROI), and corresponds to the complexity of the pixel intensity associated with the ROI, which is analogous to a fractal surface. We show that the measure is useful in characterizing immunofluorescent staining patterns, and apply this measure to study the effects of ethanol exposure on μ-calpain and calpastatin-associated immunoreactivity. Exposure of PC12 cells to ethanol (80 mM) × 48 h resulted in alterations in immunofluorescent signal (Control vs ethanol) associated with actin, calpastatin and μ-calpain: 2289 ± 166 vs 1709 ± 69, $P < 0.01$; 1681 ± 38 vs 2224 ± 95, $P < 0.001$; 1823 ± 39 vs 2841 ± 68, $P < 0.0001$ respectively, magnitudes being pixel intensity units on a scale of 0–4095. D-values for the three proteins in the same order were: 2.32 ± 0.01 vs 2.31 ± 0.03, NS; 2.31 ± 0.01 vs 2.32 ± 0.01, NS; 2.16 ± 0.03 vs 2.24 ± 0.02, $P < 0.01$, with a possible D-value range of 2–3. © 2000 Published by Elsevier Science B.V.

Keywords: Fractal; Calpain; Calpastatin; Actin; Alcohol; Ethyl

1. Introduction

Fractal geometry, pioneered by Benoit Mandelbrot (1988), underlies a set of powerful analytic tools that allow many natural and biological phenomena heretofore resistant to mathematical description to be characterized. In the field of neurohistochemistry, these tools have proven useful in the morphological analysis of neurons in cell culture. The complexity of the cell borders and outlines of neural processes are reliably parameterized using fractal measures. An excellent review of this subject has been presented (Smith et al., 1996).

Fractal methods have been used to quantitate the morphological features of one-bit binary images derived from various cell types. In this study, the area of interest is a perimeter such as the border of a cell or nucleus, or branched dendrites of neurons or glial processes (Caserta et al., 1990, 1992, 1995; Reichenbach et al., 1992). After appropriate filtering to detect edges (Smith et al., 1988), a reasonable threshold value can be estimated since the structure of interest is known a priori. The resulting one-bit image retains the spatial information of interest (Sedivy et al., 1999; Dioguardi et al., 1999). This technique has also been applied to characterize the atypia of cell nuclei (Losa et al., 1999; Sedivy et al., 1999)

We are interested in characterizing the immunofluorescent staining patterns of calcium-activated proteins such as calpain, and their endogenous in-

* Correspondence author. Tel.: +1-301-4969420; fax: +1-301-4020445.

E-mail address: pbdp@helix.nih.gov (P.B. DePetrillo).

0165-0270/00/$ - see front matter © 2000 Published by Elsevier Science B.V.
PII: S0165-0270(00)00317-4

hibitor, calpastatin in PC12 cells. Previously, we had shown that ethanol exposure decreased PC12 calcium-activated calpain activity (DePetrillo, 1997). However, the absolute cellular levels of the proteases, m-calpain and μ-calpain, and calpastatin were not found to be significantly altered using immunoblotting methods. We therefore addressed whether cellular localization of these proteases, and their endogenous inhibitor, calpastatin, was altered by ethanol exposure. Shifts in intracellular localization of the proteins would likely alter immunofluorescent staining patterns. Such changes in staining patterns in the absence of alteration in overall cellular levels of the proteases and/or their inhibitor might underlie the effects of ethanol exposure on protease activity.

In previous experiments, it was noticed that the after ethanol exposure, immunofluorescent signal associated with μ-calpain immunoreactivity was increased, and the pattern of staining had a more granular texture. The objective quantization of these patterns, altered in response to experimental treatments, was therefore the primary focus of this work. It was hypothesized that these qualitative differences in staining patterns were amenable to fractal decomposition which would provide us with an objective method of determining the magnitude of this effect. In the current set of experiments, we also probed for an unrelated cytoskeletal protein, actin, as a control for possible non-specific ethanol-related effects.

2. Materials and methods

2.1. Computation of fractal parameter

Digital representations of photomicrographic images can be conceived as fractal landscapes, the x–y axes defining the pixel location on a plane, and the z-axis value associated with pixel intensity or 'height.' It was shown by Sayles and Thomas (1978) that for a surface, a measure of surface roughness can be determined from the variance:

$$\sigma^2 = \langle z(x)^2 \rangle. \tag{1}$$

The height of the surface, z being measured as a function of the distance x along some direction, with the brackets signifying that the measurements are an average over a set of repeated observations along many discrete areas of the surface of interest. In the same report, it was also shown that the variance of z of these surfaces increases with the size of the surface. Berry and Hannay (1978) developed the idea that for naturally occurring surfaces which have no scale, have spectra of the form:

$$G(f) = \frac{k}{f^{-2H-1}}. \tag{2}$$

Here, $G(f)$ is the power-spectral intensity as defined by a Fourier transform. Mandelbrot (1988) pointed out that the Hurst exponent (H) appearing here is related to the surface fractal dimension D:

$$D = 3 - H, \tag{3}$$

where $0 < H < 1$ and $2 < D < 3$. As the complexity of the surface increases, fractionally 'filling' the third dimension, D approaches the value of 3.

An alternative way to directly examine the dependence of the surface variance on area size which does not require a Fourier transform is to derive a function which directly relates surface height variance to area size. If this relationship exists then there should be a scaling factor relating area size to variance. The method is closely related to dispersional analysis as described by Bassingthwaighte and involves measuring the variance of a signal, in this case pixel intensity, at successively different levels of resolution (Bassingthwaighte and Raymond, 1995).

For any particular size area $A[n]$ defined by the pixel number n, the standard deviation of the pixel intensity S.D.$[n]$ is calculated. If the standard deviation of the pixel intensity follows a power law relationship, then the variance will vary as a power of the area size, $A[n]$:

$$\text{S.D.}[n] = C(A[n])^S, \tag{4}$$

C is a constant, and S is an exponential parameter. We can also represent the same relationship where we substitute $D-2$ for S. This substitution is made so that the parameter D, which is the fractal dimension D_f, conforms to its scaling role in the power law relationship for a two dimensional surface:

$$\text{S.D.}[n] = C\left(\frac{A(n)^D}{A(n)^2}\right), \quad 2 < D < 3. \tag{5}$$

When $D > 2$, the variance increases as a power function of the area size $A[n]$. The parameter D is a measure of the 'roughness' of the surface, as it extrudes into a third dimension. When $D \to 2$, the surface is smoother. Its fractal dimension D approaches the spatial dimension which it occupies. As $D \to 3$, the surface convolutions begin to fill the three dimensional space. A linearized version of Eq. (5) is used to determine D as the slope of a log–log plot:

$$\log(\text{S.D.}[n]A[n]^2) = C + D\ \log(A[n]). \tag{6}$$

Several predictions follow from this relationship. For areas in which pixel intensity is not spatially correlated, D should approach 2, as expected from an ROI taken from the background. In this case, the pixel intensity varies randomly based on the operating characteristics of the image capture device as well as procedural variance in signal due to, for example, differences in

background retention of primary and/or secondary antibody.

2.2. Experimental procedures

The following reagents were used. PC12 cells derived from a rat pheochromocytoma line (American type Culture Collection, Manassas, VA, USA). RPMI 1640, heat-inactivated horse serum, fetal bovine serum and gentamicin (Life Technologies, Rockville, MD); antibody to μ-calpain (Affinity Bioreagents, Inc. Golden, CO); FITC-coupled secondary antibodies (Jackson ImmunoResearch, West Grove, PA); 0.01% Poly-L lysine and sodium borohydride (Sigma, St. Louis, MO); Permanox chamber slides (NUNC, Rochester, NY); 0.5 M EDTA (Digene, Gaithersburg, MD); ethyl alcohol (Fisher Scientific, Suwanee, GA). The anti-calpastatin polyclonal antibody was generated in rabbits using a synthetic peptide corresponding to amino-acid subunits (KLGERDDTIPPEYRHLLD) of rat calpastatin (GENBANK ACCESSION X56729).

2.2.1. Cell culture

PC12 cells were grown in RPMI 1640 with L-glutamine supplemented with 10% inactivated horse serum, 5% fetal bovine serum and 50 μg/ml gentamicin. Cells were incubated in a humidified incubator at 37°C, 5% CO_2, until confluent. Cells were harvested from the Falcon flasks by exposure to 2 mM EDTA for 10 min at 37°C. The cells were re-plated onto Permanox chamber slides coated with 0.01% Poly-L-lysine at the density of 5000/ml. The cells were treated 80 mM ethanol × 48 h prior to fixation and staining.

2.2.2. Immunofluorescent histochemical procedures

Permanox chamber slides were washed ×1 with phosphate-buffered saline (PBS), and fixed for 3 min in methanol prechilled with dry ice. The wells were removed and the slides were airdried for approximately 30 s until methanol had completely evaporated. Slides were incubated in freshly prepared 0.1% sodium borohydride-PBS solution at room temperature for 30 min. After rinsing with PBS ×1, slides were blocked for 1 h by incubation with 3% normal goat serum. All slide incubations were performed in a humidified box at room temperature. Dilutions for the primary antibodies were as follows: μ calpain (1:250) calpastatin (1:100), actin (1:100) and for secondary antibodies (1:250). Slides were incubated for 1 h in the presence of 1% NGS in PBS and primary antibody, followed by three rinses in PBS for 5 min each and incubation with secondary antibodies, either anti-mouse or anti-rabbit, under the same conditions but in a light-impermeant box. Slides were washed ×4 with water for 10 min/wash. Slides were mounted after application of mounting medium, and imaged with an epi-fluorescence microscope (ZEISS Axioskop, Thornwood, NY). Images were obtained using with a 63×/1.25 objective using a Sensys (Photometrics, Munich, DE) cooled-CCD camera and IPlab (Scanalytics, Fairfax, VA) imaging software controlled by a G4 (Apple, Cupertino, CA) computer.

After capture, the 16-bit image was saved in TIFF format and imported into NIH Image for subsequent analysis. Images were analyzed in 16 bit format for densitometry and fractal analysis. Median pixel density values are reported in 8-bit format (0–255).

2.3. Data analysis

Calculations of mean pixel intensity and D were performed within NIH Image. The macro used for these calculations, as well as some test images, are available at ftp://helix.nih.gov/ pbdp/. The macro routine estimates the local fractal dimension D of a particular area of the image. To obtain an unbiased estimate of D because of the multifractal nature of the image which will be discussed below, D is calculated as the average of a series of slopes estimated by successively collapsing a rectangular area of size $A[n]$ along eight different axes, as well as from the perimeter towards the center. In the first routine the Area[n] is collapsed along both the x- and y-axes one pixel at a time as long as $n > 9$. In the second through the fifth routines, the rectangle is anchored to each of the four vertices, and the area is collapsed by one pixel row and column width with each iteration. In the sixth through the ninth routines, the four sides of the rectangle are fixed in succession, and the area is collapsed one row and one column width towards the fixed side, with the midpoint of the anchored side serving as the anchor. S.D.[n] is calculated for the original areas and for each iteration of the new collapsed areas. The results of this procedure were fit to Eq. (6) using a simple least-squares linear regression fit. The program output gives the mean slope D and its standard error based on the parameters of the fit. The output also includes the mean intensity of the ROI.

We obtained one estimate of each parameter of interest from each image by averaging the results from 1 to 6 individual cells per field. We examined at least 6–12 different images for each experimental condition. Values were compared and contrasted using the Mann–Whitney U test, since we did not assume normality.

3. Results

The R-value for the linear regressions used for the calculation of D values were all > 0.95, suggesting that a strong scale-independent power law relationship (Peitgen et al., 1992) between the area $A[n]$ and the S.D.[n]

exists and applies to ROIs located in the background, or within areas encompassing cellular structures. Values of D obtained from 25 × 25 pixel background areas from our images are typically in the range of 2.02–2.06, as expected.

To evaluate the method using synthetically generated non-spatially correlated data, an image of 100 × 100 pixels was generated by sampling synthetic intensity values obtained from a Gaussian distribution with a mean of 200 and a standard deviation of 1. These values are similar to those obtained from background samples with a pixel intensity scale of 0–255. For a randomly selected 25 × 25 pixel area within this 100 × 100 pixel area space, we obtained the expected result of $D = 1.997 \pm 0.004$, $R = 0.999$ for the regression.

The distribution of D-values obtained for ROI from cellular images was examined using normal probability plots to check for deviations from normality (Van Der Kloot, 1991). The results are presented in Fig. 1. The distribution of the fractal dimension D of the ROI is shown to have an approximate normal distribution.

The effects of arithmetically varying pixel intensity values on the magnitude of the calculated D was examined, using experimentally derived image data. Linear alterations in pixel intensity were not expected to alter the value of D, since D is a measure of surface complexity. In Table 1, we show the results of mean intensity and FD for the same ROI. The pixel densities of the original 16-bit image were increased and decreased by 400, 800 and 1600. The original values were obtained from a 25 × 25 pixel area in a cell stained for calpastatin immunoreactivity.

The result shows no variation in the value of D over a large range of pixel intensities. Similar results are obtained when the ROI encompasses regions of higher or lower values of D, where the variation in D is typically less than 0.4%.

Correlates of the ROI pixel histogram values and D are shown in Fig. 2. The histogram of the background shows a narrow gaussian distribution, with an associated D-value of 2.05 ± 0.01, close to the expected value of 2.00, suggesting there is very little spatial correlation between pixel intensity values. This is supported by the observation that the distribution of pixel intensity is gaussian.

Images obtained using anti-μ-calpain, anti-calpastatin, and anti-actin were examined before and after exposure to 80 mM ethanol × 48 h. Measurement results for mean intensity and D are in Table 2 and represented in Fig. 3. The distribution of the intensity measurements was normal. Results for intensity measurements could have therefore been compared using a parametric ANOVA. However, we chose the more conservative non-parametric Mann–Whitney U test for all comparisons of values from control vs ethanol-exposed conditions.

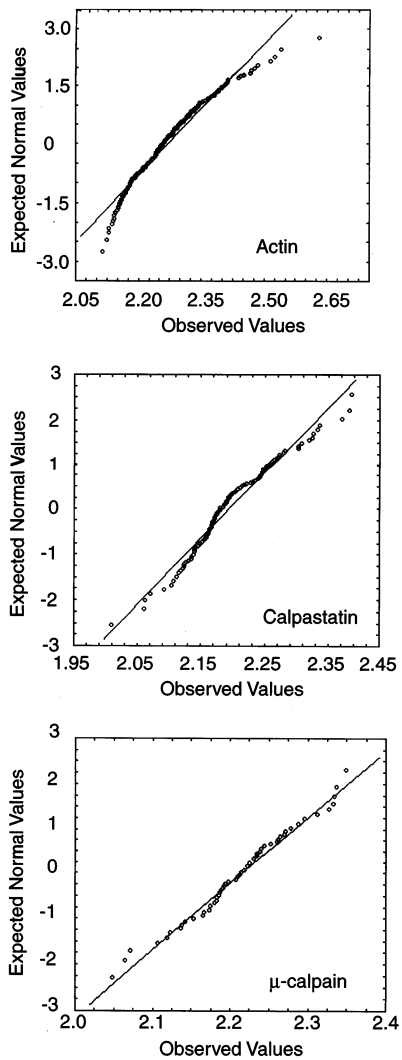

Fig. 1. Normal probability plots of fractal intensity parameter D obtained for slides stained with actin, calpastatin, and μ-calpain antibodies under control conditions.

4. Discussion

We have shown that the fractal dimension parameter, D, can be used to measure the spatial variation of intensity values in immunofluorescently stained cells. The measure allows us to objectively quantitate the

Table 1
Fractal dimension and intensity

Pixel intensity adjustment	Mean pixel intensity	D
+1600	3401.39	2.30
+800	2601.39	2.30
+400	2201.39	2.30
0 (Original)	1801.37	2.30
−400	1401.35	2.30
−800	1001.35	2.30
−1600	201.35	2.30

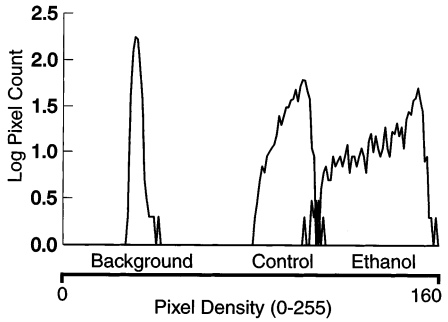

Fig. 2. Histogram of pixel intensity units with a scale of 0–255 obtained using NIHImage. The images are scaled from 0 to 255 rather than 0–4095 as they were obtained directly from NIHImage histogram plots. μ-Calpain primary antibody-related signal is shown. All pixel histograms are calculated for a 25 × 25 pixel area ROI. The pixel histogram of the background ROI taken from the control image has a narrow Gaussian shape with $D = 2.05 \pm 0.01$, close to the expected value of 2.00. Cytoplasmic ROIs from control-exposed cells result in $D = 2.16 \pm 0.03$, whereas ethanol (80 mM × 48 h) exposed cells result in $D = 2.24 \pm 0.02$. The increase in D is reflected by the increased skewness of the histogram, which is associated with the increased complexity of the intensity-surface.

degree of spatial variation in intensity which could previously only be subjectively noted. Visually, ROIs with values of $D > 2$ exhibit heterogeneous staining patterns consistent with visualization of structural components within the cytoplasm. Diffuse, structureless patterns result in D values close to two. This can be readily seen by examining Fig. 4, where the pattern associated with anti-calpastatin staining under both experimental conditions has a more granular texture than that seen with staining observed with anti-μ-calpain. These differences are reflected in higher D-values for anti-calpastatin vs. anti-μ-calpain, as shown in Fig. 3. The distinct granular texture of anti-calpastatin staining in PC 12 cells has also been demonstrated by (Tullio et al., 1999) in studies employing similar immunofluorescent histochemical techniques.

The current method is shown to resolve differences in immunofluorescent staining that may not be apparent if parameterized by signal magnitude alone. For example, μ-calpain associated immunoreactivity as measured by intensity is altered by ethanol exposure, but unlike calpastatin- or actin-associated immunoreactivity, the pattern of staining is also affected. Ethanol exposure resulted in a higher D value, suggesting that μ-calpain associated immunoreactivity is spatially altered in ethanol treated cells.

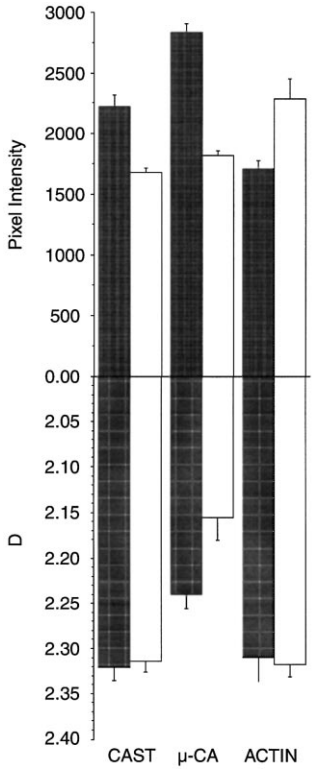

Fig. 3. Intensity measurements (top of figure) and D-values (bottom of figure) obtained from PC12 cytoplasm stained with the respective primary antibody: CAST, calpastatin; μ-CA, μ-calpain; and ACTIN, alpha-actin. For both top and bottom, the height of the bars represents the mean intensity measure or the D-values of $n = 6$–12 images each sampled 4–8 times with the distal line showing the positive displacement of the SEM. The dark and light colorings are associated with measurements obtained from ethanol (80 mM × 48 h) and control conditions respectively. Intensity was measured on a scale of 0–4095, inverted so that pixel intensity was inversely correlated with fluorescent signal intensity. Significant differences in mean intensity are present between ethanol and control conditions for all three proteins, at $P < 0.001$, $P < 0.0001$, and $P < 0.01$ for CAST, μ-CA, and ACTIN respectively. In the lower portion, measurements of D, a dimensionless constant where $2 < D < 3$ are shown. The only significant difference in D-values between ethanol and control conditions is obtained with μ-CA, at $P < 0.01$.

Table 2
Experimental results

	Calpastatin		μ-Calpain		Actin	
	Control	Ethanol	Control	Ethanol	Control	Ethanol
Intensity ± SEM	1681 ± 38	2224 ± 95	1823 ± 39	2841 ± 68	2289 ± 166	1709 ± 69
P-value	0.001		0.0001		0.01	
D ± SEM	2.31 ± 0.01	2.32 ± 0.01	2.16 ± 0.03	2.24 ± 0.02	2.32 ± 0.01	2.31 ± 0.03
P-value	NS		0.01		NS	

Evidence that calpain localization is shifted in response to factors that alter enzymatic activity is well known, and may be associated with this alteration in staining pattern (Pontremoli et al., 1989; Neuberger et al., 1997). Protein shifts within cellular domains are often associated with concomitant changes in either gross localization or in more subtle shifts in staining patterns characterized as diffuse or granular.

The variation in calpastatin immunoreactivity, along with alterations in calpain-related immunoreactivities suggests that the decrease in calpain related protease activity in PC12 cells may be related to either a change in a protein–protein interaction that uncovers an epitope on the protein available for IgG binding, or that the ethanol exposure may induce a change in the localization of the proteins, resulting in altered immunoreactivity.

While we expected to find little or no change in actin immunoreactivity, actin immunoreactivity decreased after exposure to ethanol but the fractal parameter D was unchanged. These results suggests that the ethanol alters immunohistochemical reactivity in a protein-specific manner and does not alter its spatial relationships within the cell.

Many biological structures are multi-fractal, meaning that the scaling exponent, or D, is not fixed over a wide dynamic range of scales. The shape of the curve relating scale to variance may change abruptly, especially at the highest and lowest degrees of resolution. The method will therefore produce biased results if ROIs are analyzed that exhibit high degrees of multifractality. For example, this would occur if an ROI is chosen which includes a nucleus-cytoplasm interface, where D associated with nuclear staining is very different from D associated with cytoplasmic staining. If such areas are chosen for analysis, the resulting D value will have a higher associated error, reflecting an increase in the variance of the least squares fit. These estimation errors are avoided by choosing ROIs for analysis that do not encompass regions with obvious major changes in staining pattern. For example, ROIs that include background as well as cytoplasm, or cytoplasm as well as nucleus should be avoided.

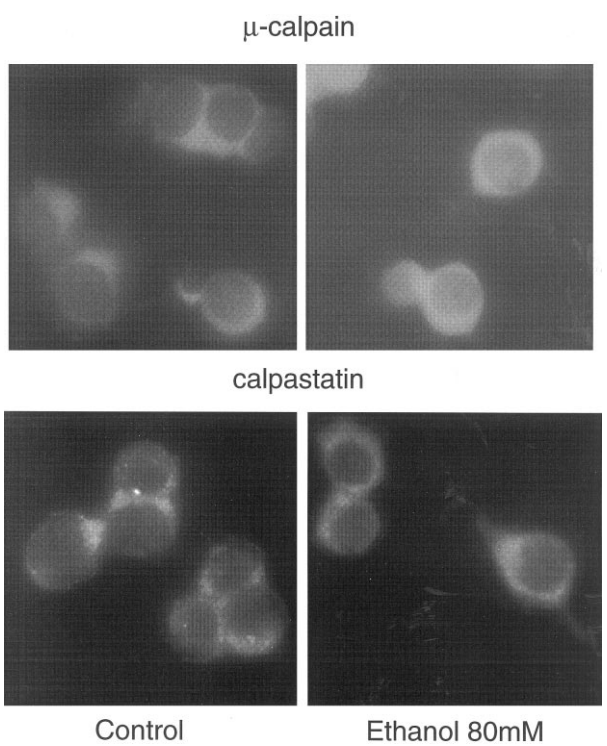

Fig. 4. Images of control and ethanol-exposed (80 mM × 48 h) cells stained with anti-μ-calpain or anti-calpastatin primary antibodies and FITC-coupled secondary antibody.

The estimate of D was obtained along eight axes and by collapsing the area towards the center so as to minimize the bias introduced by the multifractal nature of the surface. During the iterative process, areas occasionally collapse around a set of very bright or dark pixels. Therefore, if D was estimated using only one linear regression, bias could occur especially at smaller area-related measurements of the standard deviation of pixel intensity.

One of the strengths of this method is that it could be adapted to calculate D for three dimensional sections such as may result from a confocal image, since the standard deviation of voxel intensity could be determined by collapsing a volume, rather than an area. In theory, the same general mathematical decomposition applied to volume rather than area should result in a fractal parameter with a value between 3 and 4, one dimension higher than the current method.

Since the method allows the computation of D of a surface, any image where there exists a spatial correlation between pixel intensities should be amenable to analysis. This may include, but is not limited to groups of cells such as neurons that exhibit non-random spatial correlations. In these cases, the non-random pattern of cell growth may be imaged as a complex surface that might be characterized by the parameter, D. This might be applicable to the study of phenomena such as neurite outgrowth.

Currently, we are adapting this method to allow the quantization of the fractal parameter D for irregularly shaped areas to allow complete sampling of regions such as nucleus or cytoplasm. The current method is limited by its dependence on the collapse of a rectangular area which is placed within an area of interest.

In summary, we have shown that immunofluorescent images can be analyzed as fractal surfaces where the height of the surface corresponds to pixel intensity. The resultant fractal parameter, D, is a useful measure of the pattern of staining. The measure results in an approximately normally distributed parameter, D, which is amenable to statistical comparisons. The

parameter is not sensitive to arithmetic variations in pixel intensity between experiments, which further enhances it usefulness for comparative studies.

Acknowledgements

The authors wish to thank Erick D. Singley for technical help related to installation and testing of the imaging software and controllers, and an anonymous reviewer for the suggestion of using normal probability plots to examine the normality of the derived *D* parameter. This research was supported by the Intramural Research Funds from the National Institute on Alcohol Abuse and Alcoholism

References

DePetrillo PB. Calcium-activated neutral protease activity is decreased in PC12 cells after ethanol exposure. J Neurochem 1997;68:1863–9.

Bassingthwaighte JB, Raymond GM. Evaluation of the dispersional analysis method for fractal time series. Ann Biomed Eng 1995;23:491–505.

Caserta F, Stanley HE, Eldred WD, Daccord G, Hausman RE, Nittman J. Physical mechanisms underlying neurite outgrowth. Phys Rev Lett 1990;64:95–8.

Caserta F, Hausman RE, Eldred WD, Kimmel C, Stanley HE. Effect of viscosity on neurite outgrowth and fractal dimension. Neurosci Lett 1992;136:198–202.

Caserta F, Eldred WD, Fernandez E, Hausman RE, Stanford LR, Bulderev SV, et al. Determination of fractal dimension of physiologically characterized neurons in two and three dimensions. J Neurosci Methods 1995;56:133–44.

Dioguardi N, Grizzi F, Bossi P, Roncalli M. Fractal and spectral dimension analysis of liver fibrosis in needle biopsy specimens. Analyt Quant Cytol Histol 1999;21:262–6.

Losa GA, Graber R, Baumann G, Nonnenmacher TF. Effects of steroid hormones on nuclear membrane and membrane-bound heterochromatin from breast cancer cells evaluated by fractal morphometry. Analyt Quant Cytol Histol 1999;21:430–6.

Mandelbrot BB. Fractal Geometry of Nature. New York: Freeman, 1988.

Neuberger T, Chakrabarti AK, Russell T, DeVries GH, Hogan EL, Banik NL. Immunolocalization of cytoplasmic and myelin m-calpain in transfected Schwann cells: I. Effect of treatment with growth factors. Neurosci Res 1997;47:521–30.

Pontremoli S, Melloni E, Salamino F, Patrone M, Michetti M, Horecker BL. Activation of neutrophil calpain following its translocation to the plasma membrane induced by phorbol ester or fMet-Leu-Phe. Biochem Biophys Res Commun 1989;160:737–43.

Reichenbach A, Siegel A, Senitz D, Smith TG. A comparative fractal analysis of various mammalian cell types. Neuroimage 1992;1:69–72.

Sayles RS, Thomas TR. Surface topography as a nonstationary random process. Nature 1978;271:431–4.

Sedivy RS, Windishberger C, Svozil K, Moser E, Breitenecker G. Fractal analysis: an objective method for identifying atypical nuclei in dysplastic lesions of the cervix uteri. Gynecol Oncol 1999;75:78–83.

Smith TG, Marks WB, Lange GD, Sheriff WH, Neale EA. Edge detection in images using Marr-Hildreth filtering techniques. J Neurosci Methods 1988;26:75–82.

Smith TG, Lange GD, Marks WB. Fractal methods and results in cellular morphology-dimensions, lacunarity and multifractals. J Neurosci Methods 1996;69:123–36.

Tullio RD, Passalacqua M, Averna M, Salamino F, Melloni E, Pontremoli S. Changes in intracellular localization of calpastatin during calpain activation. Biochem J 1999;343:467–72.

Van Der Kloot W. The regulation of quantal size. Prog Neurobiol 1991;36:93–130.